

Algebraic proof and application of Lumley's realizability triangle

G.A. Gerolymos and I. Vallet

Sorbonne Universités, Université Pierre-et-Marie-Curie (UPMC), 4 place Jussieu, 75005 Paris, France
Emails: georges.gerolymos@upmc.fr, isabelle.vallet@upmc.fr

Lumley [Lumley J.L.: *Adv. Appl. Mech.* **18** (1978) 123–176] provided a geometrical proof that any Reynolds-stress tensor $\overline{u'_i u'_j}$ (indeed any tensor whose eigenvalues are invariably nonnegative) should remain inside the so-called Lumley's realizability triangle. An alternative formal algebraic proof is given that the anisotropy invariants of any positive-definite symmetric Cartesian rank-2 tensor in the 3-D Euclidian space \mathbb{E}^3 define a point which lies within the realizability triangle. This general result applies therefore not only to $\overline{u'_i u'_j}$ but also to many other tensors that appear in the analysis and modeling of turbulent flows. Typical examples are presented based on DNS data for plane channel flow.

1 Introduction

The introduction in [10] of Lumley's [9] realizability triangle is without doubt one of the most important contributions to statistical turbulence theory. The Reynolds-stress tensor property that serves to prove that every possible (realizable) Reynolds-stress tensor should lie within Lumley's [9] realizability triangle, is the positivity of the diagonal components of the covariance of velocity-fluctuations

$$r_{ij} := \overline{u'_i u'_j} \quad (1a)$$

in every reference-frame, and hence also in the frame of its principal axes [9], implying that the tensor $\overline{u'_i u'_j}$ is positive-definite [15, Theorem 2.3, p. 186], is exactly the same as that behind Schumann's [11] realizability conditions. Throughout the paper, $u_i \in \{u, v, w\}$ are the velocity components in a Cartesian coordinates system $x_i \in \{x, y, z\}$, ν is the kinematic viscosity, $(\cdot)'$ denotes Reynolds (ensemble) fluctuations and (\cdot) denotes Reynolds (ensemble) averaging.

Lee and Reynolds [8] further argued that Lumley's [9] realizability triangle also applies to the dissipation tensor

$$\varepsilon_{ij} := 2\nu \overline{\frac{\partial u'_i}{\partial x_k} \frac{\partial u'_j}{\partial x_k}} \quad (1b)$$

and to the covariance of the fluctuating vorticity components

$$\zeta_{ij} := \overline{\omega'_i \omega'_j} \quad (1c)$$

where ω'_i are the fluctuating vorticity components. Obviously the diagonal components of both these tensors are positive for every orientation of the axes of the Cartesian coordinates system.

Realizability constraints are essential not only in theory and modelling [9, 10] but also in computational implementations of second-moment closures [2, 3]. The same positivity of the diagonal components for every orientation of the axes of coordinates, which is equivalent to the positive-definiteness of the symmetric real tensor [15, Theorem 2.2, p. 186], and implies Lumley's [9] realizability triangle, can also be of interest to the unresolved stresses [14] in partially-resolved approaches [6].

Lumley's [9] proof of the realizability triangle is geometric, based on representing the behaviour of 2 of the principal values of the traceless anisotropy tensor, and taking into account the corresponding behaviour of the invariants. An alternative easy-to-follow algebraic proof is possible, based on just 2 requirements

1. the symmetric Reynolds-stress tensor has 3 real eigenvalues [12, Theorem 2, p. 55]
2. which are nonnegative [9, 11] with nonzero trace (positive kinetic energy)

which also apply to any symmetric real positive-definite rank-2 tensor in \mathbb{E}^3 .

2 Anisotropy, principal axes and invariants

Before giving the proof, we summarize for completeness some basic definitions and properties [9, 12]. The tensor of the 2-moments of fluctuating velocities r_{ij} (1a) is real and symmetric, and is therefore diagonalizable in the frame of its principal axes [12, Theorem 5, p. 59], where its diagonal components (principal values) are its real [12, Theorem 2, p. 55] eigenvalues [12, Theorem 4, p. 58]. This implies that the eigenvalues of \mathbf{r} , being its diagonal components in

the frame of its principal axes, are nonnegative. Since the eigenvalues of the symmetric tensor \mathbf{r} are nonnegative, \mathbf{r} is positive-semidefinite [15, Theorem 2.3, p. 186]. Inversely, the diagonal components of every positive-semidefinite tensor are nonnegative [15, p. 186]. The halftrace of \mathbf{r} is the turbulent kinetic energy and is therefore nonzero ($\text{tr}\mathbf{r} = 2k > 0$), implying that at least one of its eigenvalues is nonzero (therefore \mathbf{r} is positive-definite, which inversely implies nonzero trace). Let $\mathbf{\Lambda}_{\mathbf{r}}$ and $\mathbf{\Lambda}_{\mathbf{b}_r}$

$$\mathbf{\Lambda}_{\mathbf{r}} := \begin{bmatrix} \lambda_{r1} & 0 & 0 \\ 0 & \lambda_{r2} & 0 \\ 0 & 0 & \lambda_{r3} \end{bmatrix} ; \quad \mathbf{\Lambda}_{\mathbf{b}_r} := \begin{bmatrix} \lambda_{br1} & 0 & 0 \\ 0 & \lambda_{br2} & 0 \\ 0 & 0 & \lambda_{br3} \end{bmatrix} \quad (2a)$$

be the diagonal matrices of the eigenvalues of \mathbf{r} and \mathbf{b}_r , respectively, where

$$\mathbf{b}_r := \frac{\mathbf{r}}{\text{tr}\mathbf{r}} - \frac{1}{3}\mathbf{I}_3 \implies \begin{cases} \text{I}_{\mathbf{b}_r} = \text{tr}\mathbf{b}_r = 0 \\ \text{II}_{\mathbf{b}_r} = -\frac{1}{2}b_{rij}b_{rji} \\ \quad = -\frac{1}{2}\lambda_{bri}\lambda_{bri} < 0 \\ \text{III}_{\mathbf{b}_r} = \det\mathbf{b}_r = \lambda_{br1}\lambda_{br2}\lambda_{br3} \end{cases} \quad (2b)$$

is the traceless anisotropy tensor corresponding to \mathbf{r} and \mathbf{I}_3 is the 3×3 identity tensor, with the usual definition of the invariants [12, (6), p. 51], simplified [9] by the relation $\text{I}_{\mathbf{b}_r} = \text{tr}\mathbf{b}_r = 0$ (2b), and the corresponding expressions in terms of the eigenvalues in the frame of principal axes [9]. By definition (2b), \mathbf{b}_r is real symmetric, and has therefore real eigenvalues [12, Theorem 2, p. 55]. It is straightforward to show that the eigenvectors of \mathbf{r} are also eigenvectors of \mathbf{b}_r . Let $\mathbf{X}_{\mathbf{r}}$ and $\mathbf{X}_{\mathbf{b}_r}$ denote the orthonormal matrices [12, Theorem 5, p. 59] whose columns are the right eigenvectors of \mathbf{r} and \mathbf{b}_r , respectively, and therefore satisfy

$$\mathbf{r} \cdot \mathbf{X}_{\mathbf{r}} = \mathbf{\Lambda}_{\mathbf{r}} \cdot \mathbf{X}_{\mathbf{r}} ; \quad \mathbf{b}_r \cdot \mathbf{X}_{\mathbf{b}_r} = \mathbf{\Lambda}_{\mathbf{b}_r} \cdot \mathbf{X}_{\mathbf{b}_r} \quad (3a)$$

By straightforward computation using (2b, 3a)

$$\begin{aligned} \mathbf{b}_r \cdot \mathbf{X}_{\mathbf{r}} &\stackrel{(2b)}{=} \left(\frac{\mathbf{r}}{\text{tr}\mathbf{r}} - \frac{1}{3}\mathbf{I}_3 \right) \cdot \mathbf{X}_{\mathbf{r}} = \frac{1}{\text{tr}\mathbf{r}} \mathbf{r} \cdot \mathbf{X}_{\mathbf{r}} - \frac{1}{3}\mathbf{X}_{\mathbf{r}} \\ &\stackrel{(3a)}{=} \left(\frac{1}{\text{tr}\mathbf{r}} \mathbf{\Lambda}_{\mathbf{r}} - \frac{1}{3}\mathbf{I}_3 \right) \cdot \mathbf{X}_{\mathbf{r}} \end{aligned} \quad (3b)$$

implying by (3a)

$$\mathbf{X}_{\mathbf{b}_r} \stackrel{(3a, 3b)}{=} \mathbf{X}_{\mathbf{r}} \quad (3c)$$

$$\mathbf{\Lambda}_{\mathbf{b}_r} \stackrel{(3a, 3b)}{=} \frac{1}{\text{tr}\mathbf{r}} \mathbf{\Lambda}_{\mathbf{r}} - \frac{1}{3}\mathbf{I}_3 \iff \lambda_{ri} = (\text{tr}\mathbf{r}) \left(\lambda_{bri} + \frac{1}{3} \right) \quad (3d)$$

ie \mathbf{r} and \mathbf{b}_r have the same system of principal axes and their eigenvalues are related by (3d).

3 Proof

As stated in the introduction the algebraic proof of Lumley's [9] realizability triangle can be easily obtained from 2 well-known conditions, also discussed in (§2). The eigenvalues of \mathbf{b}_r satisfy the characteristic polynomial [12, (5), p. 51]

$$\lambda_{b_r}^3 - \underbrace{\text{I}_{\mathbf{b}_r}}_{\stackrel{(2b)}{=} 0} \lambda_{b_r}^2 + \text{II}_{\mathbf{b}_r} \lambda_{b_r} - \text{III}_{\mathbf{b}_r} = 0 \quad (4a)$$

The roots of the cubic equation (4a) are real iff [7, pp. 44–45] its determinant is nonpositive,¹ ie

$$\begin{aligned} \mathbf{b}_r \text{ has 3 real eigenvalues} &\iff \left(\frac{1}{9}(3\text{II}_{\mathbf{b}_r}) \right)^3 + \left(\frac{1}{2}\text{III}_{\mathbf{b}_r} \right)^2 \leq 0 \\ &\iff -\text{II}_{\mathbf{b}_r} \geq 3 \left(\frac{1}{4}\text{III}_{\mathbf{b}_r}^2 \right)^{\frac{1}{3}} \end{aligned} \quad (4b)$$

readily implying that possible (realizable) states must lie (Fig. 1) above the 2 branches of axisymmetric componentality in the $(\text{III}_{\mathbf{b}_r}, -\text{II}_{\mathbf{b}_r})$ -plane [13]. Furthermore, the eigenvalues of \mathbf{r} representing also its diagonal components in the system of principal axes [12, Theorem 4, p. 58] must be nonnegative, also implying that $\det\mathbf{r} = \lambda_{r1}\lambda_{r2}\lambda_{r3} \geq 0$, the last of the 3 realizability conditions of Shumann [11]. Using the relation (3d) between the eigenvalues of \mathbf{r} and \mathbf{b}_r

$$\begin{aligned} 0 &\leq \frac{1}{(\text{tr}\mathbf{r})^3} \lambda_{r1}\lambda_{r2}\lambda_{r3} \stackrel{(3d)}{=} \left(\lambda_{br1} + \frac{1}{3} \right) \left(\lambda_{br2} + \frac{1}{3} \right) \left(\lambda_{br3} + \frac{1}{3} \right) \\ &\stackrel{(2)}{=} \frac{1}{27} + \frac{1}{3}\text{II}_{\mathbf{b}_r} + \text{III}_{\mathbf{b}_r} \iff -\text{II}_{\mathbf{b}_r} \leq \frac{1}{9} + 3\text{III}_{\mathbf{b}_r} \end{aligned} \quad (5)$$

implying that possible (realizable) states equally lie (Fig. 1) below the 2-C straight line in the $(\text{III}_{\mathbf{b}_r}, -\text{II}_{\mathbf{b}_r})$ -plane [13]. The intersection of these 2 inequalities is precisely Lumley's [9] realizability triangle

$$(4b, 5) \implies 3 \left(\frac{1}{4}\text{III}_{\mathbf{b}_r}^2 \right)^{\frac{1}{3}} \leq -\text{II}_{\mathbf{b}_r} \leq \frac{1}{9} + 3\text{III}_{\mathbf{b}_r} \quad (6)$$

and is defined by the 2 conditions stated in (§1), viz that the eigenvalues of \mathbf{r} are real and positive.

Notice that (6) describes precisely a curvilinear triangle (Fig. 1), because the 2 axisymmetric branches $-\text{II}_{\mathbf{b}_r} = 3 \left(\frac{1}{4}\text{III}_{\mathbf{b}_r}^2 \right)^{\frac{1}{3}}$ (4b) are obviously described by the same single-valued function of $\text{III}_{\mathbf{b}_r}$ with a cusp at $(-\text{II}_{\mathbf{b}_r}, \text{III}_{\mathbf{b}_r}) = (0, 0)$, defining the isotropic 3-C corner [13, Fig. 4, p. 3]. The intersections of this single valued function with the straight line $-\text{II}_{\mathbf{b}_r} = \frac{1}{9} + 3\text{III}_{\mathbf{b}_r}$ (5) are the roots of $3 \left(\frac{1}{4}\text{III}_{\mathbf{b}_r}^2 \right)^{\frac{1}{3}} = \frac{1}{9} + 3\text{III}_{\mathbf{b}_r} \iff \text{III}_{\mathbf{b}_r}^3 - \frac{5}{36}\text{III}_{\mathbf{b}_r}^2 + \frac{1}{243}\text{III}_{\mathbf{b}_r} + \frac{1}{19683} = 0 \iff (\text{III}_{\mathbf{b}_r} + \frac{1}{108}) \left(\text{III}_{\mathbf{b}_r} - \frac{2}{27} \right)^2 = 0$, defining the 2 other corners, viz the 1-C corner [13, Fig. 4, p. 3] $(-\text{II}_{\mathbf{b}_r}, \text{III}_{\mathbf{b}_r}) = (\frac{1}{3}, \frac{2}{27})$ corresponding to the double root $\frac{2}{27}$ and the isotropic 2-C point [13, Fig. 4, p. 3] $(-\text{II}_{\mathbf{b}_r}, \text{III}_{\mathbf{b}_r}) = (\frac{1}{12}, -\frac{1}{108})$.

¹The cubic equation $x^3 + ax^2 + bx + c = 0$ has 3 real roots iff [7, pp. 44–45] the determinant is negative, $\Delta_3 = [\frac{1}{9}(3b - a^2)]^3 + [\frac{1}{2}(c + \frac{2}{27}a^3 - \frac{2}{27}ab)]^2 \leq 0$. If $\Delta_3 = 0$ then 2 roots are identical.

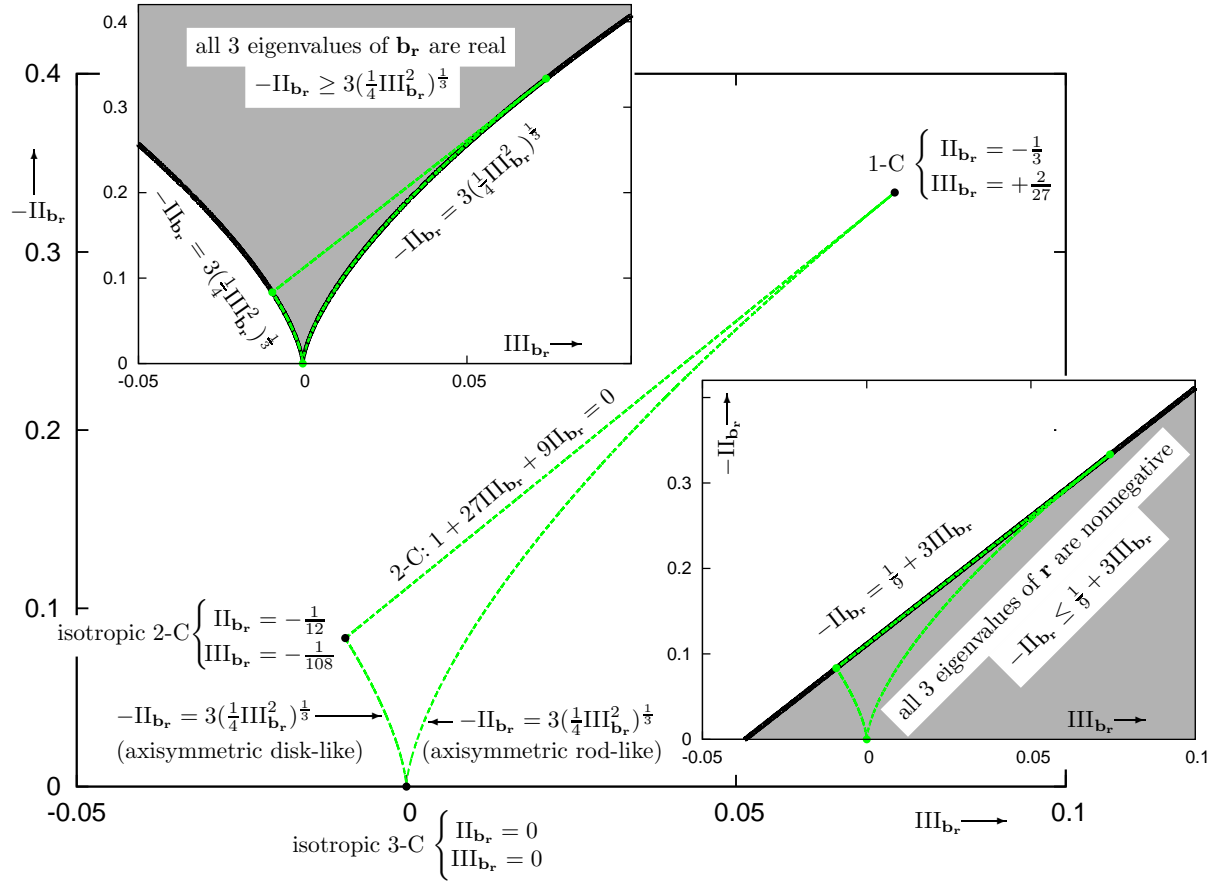


Fig. 1. Lumley's [9, 13] realizability triangle (6) for a positive-definite symmetric real rank-2 Cartesian tensor \mathbf{r} in the 3-D Euclidean space, plotted in the $(\text{III}_{\mathbf{b}_r}, -\text{II}_{\mathbf{b}_r})$ -plane of the invariants (2b) of the corresponding anisotropy tensor \mathbf{b}_r (2b), and representation of the inequalities (4b, 5) whose intersection defines the region of realizable states.

4 Applications

Obviously the property applies not only to the Reynolds-stresses r_{ij} (1a), their dissipation ε_{ij} (1b) or the vorticity covariance ζ_{ij} (1c), but also to any tensor with nonnegative diagonal values. Typical examples are the destruction-of-dissipation tensor [4, 5]

$$\varepsilon_{\varepsilon_{ij}} := 4\nu^2 \frac{\partial^2 u'_i}{\partial x_k \partial x_m} \frac{\partial^2 u'_j}{\partial x_k \partial x_m} \quad (7a)$$

which represents the destruction of ε_{ij} by the action of molecular viscosity [5, (3.3), p. 17] or the destruction-of-vorticity-covariance tensor

$$\varepsilon_{\zeta_{ij}} := 2\nu \frac{\partial \omega'_i}{\partial x_k} \frac{\partial \omega'_j}{\partial x_k} \quad (7b)$$

which represents the destruction of ζ_{ij} by the action of molecular viscosity [1, (20), p. 458].

Regarding acceleration fluctuations $(D_t u_i)'$ most authors generally study the variances of its components [17, 18] and

its splitting, based on the momentum equation, in a pressure part $\rho^{-1} \partial_{x_i} p'$ (also called *inviscid*) and a viscous part $\nu \nabla^2 u'_i$ (also called *solenoidal* because, by the fluctuating continuity equation [5, (3.2a), p. 17], it is divergence-free). As for the fluctuating vorticity correlations, we may define the symmetric positive-definite tensor of fluctuating acceleration correlations α_{ij} and the corresponding inviscid and solenoidal parts

$$\alpha_{ij} := \overline{\left(\frac{Du_i}{Dt} \right)' \left(\frac{Du_j}{Dt} \right)'} \quad (7c)$$

$$\alpha_{ij}^{(p)} := \frac{1}{\rho^2} \frac{\partial p'}{\partial x_i} \frac{\partial p'}{\partial x_j} \quad (7d)$$

$$\alpha_{ij}^{(v)} := \nu^2 \frac{\partial^2 u'_i}{\partial x_m \partial x_m} \frac{\partial^2 u'_j}{\partial x_k \partial x_k} \quad (7e)$$

We consider DNS results of fully developed (streamwise invariant in the mean) turbulent plane channel flow [4, 5], in a streamwise \times wall-normal \times spanwise $L_x \times L_y \times L_z = 4\pi\delta \times 2\delta \times \frac{4}{3}\pi\delta$ computational box, and use standard definitions [5, §3.2, p. 18] of computational parameters (Figs. 2, 3).

$$\begin{array}{cccccccccccccccc}
Re_{\tau_w} & N_x \times N_y \times N_z & L_x \times L_y \times L_z & \Delta x^+ & \Delta y_w^+ & N_{y^+ \leq 10} & \Delta y_{CL}^+ & \Delta z^+ & \Delta t^+ & t_{OBS}^+ & \Delta t_s^+ \\
180 & 401 \times 201 \times 401 & 4\pi\delta \times 2\delta \times \frac{4}{3}\pi\delta & 5.7 & 0.22 & 26 & 3.1 & 1.9 & 0.0060 & 818 & 0.0060
\end{array}$$

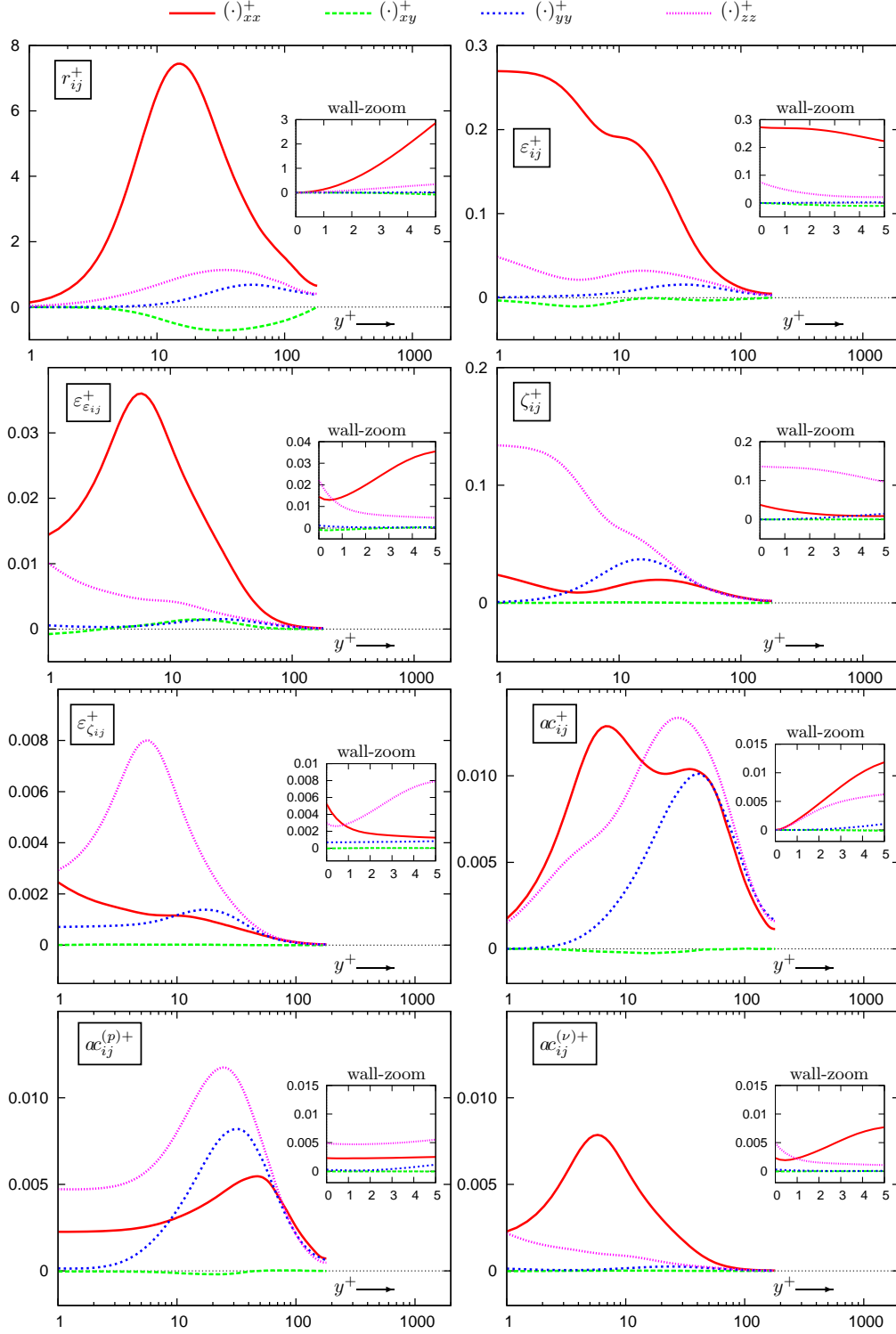


Fig. 2. Components, in wall-units [5, (A3), p. 28], of the positive-definite symmetric tensors (1, 7), plotted against the inner-scaled wall-distance y^+ (logscale and linear wall-zoom), from DNS computations of turbulent plane channel flow [4, 5].

Regarding r_{ij} (1a), its dissipation-rate ϵ_{ij} (1b) and the destruction of that dissipation $\epsilon_{\zeta ij}$ (7a), notice that the shear component $(\cdot)_{xy}$ is generally of the order-of-magnitude of the wall-normal component $(\cdot)_{yy}$ (Fig. 2). Sufficiently far

from the wall [8] r_{ij} is expected to reflect the anisotropy of the large turbulent scales (typical size ℓ_T), whereas ϵ_{ij} is expected to reflect the anisotropy of the smaller scales (of the order of the Taylor microscale λ). The scaling arguments of

$$\begin{array}{cccccccccccccccc}
Re_{\tau_w} & N_x \times N_y \times N_z & L_x \times L_y \times L_z & \Delta x^+ & \Delta y_w^+ & N_{y^+ \leq 10} & \Delta y_{CL}^+ & \Delta z^+ & \Delta t^+ & t_{OBS}^+ & \Delta t_s^+ \\
180 & 401 \times 201 \times 401 & 4\pi\delta \times 2\delta \times \frac{4}{3}\pi\delta & 5.7 & 0.22 & 26 & 3.1 & 1.9 & 0.0060 & 818 & 0.0060
\end{array}$$

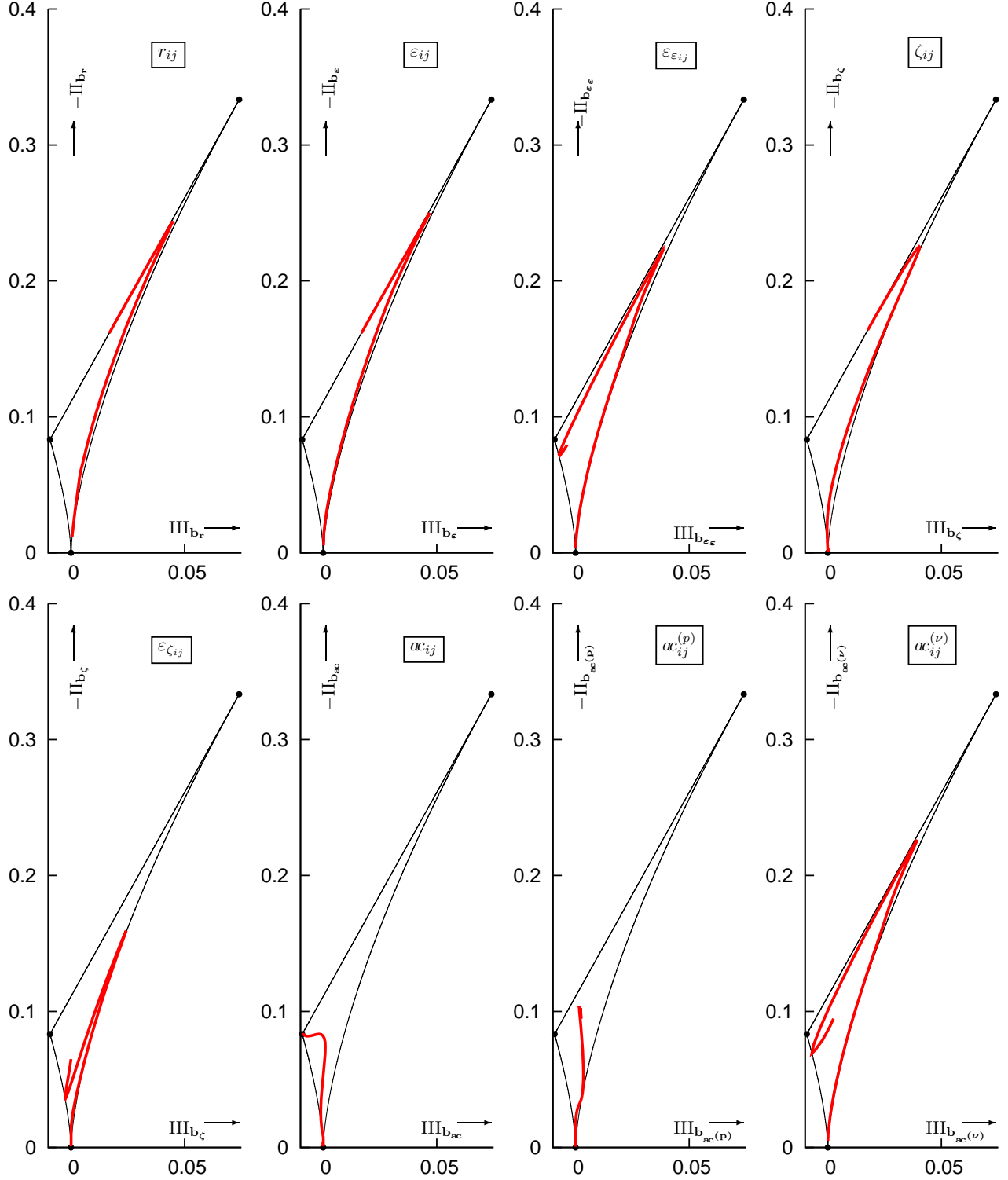


Fig. 3. Locus, within Lumley's [9, 13] realizability triangle (6) in the $(III, -II)$ -plane, of the anisotropy invariants (2b) of the positive-definite symmetric tensors (1, 7), from DNS computations of turbulent plane channel flow [4, 5].

Tennekes and Lumley [16, pp. 88–92] suggest that, again sufficiently far from the wall, ϵ_{ij} reflects the anisotropy of scales between λ and the Kolmogorov scale ℓ_K . It is therefore noteworthy that they appear to share a seemingly similar

anisotropy $(\cdot)_{xx} > (\cdot)_{zz} > (\cdot)_{yy} \forall y^+ \gtrsim 1$ (Fig. 2). Nonetheless, very near the wall ($y^+ \lesssim 1$; Fig. 2), where all these length-scales collapse to 0, ϵ_{zz} becomes larger than ϵ_{xx} . Vorticity covariance ζ_{ij} (1c) is expected [16, pp. 88–92] to reflect the

anisotropy of the same scales as ϵ_{ij} , and its destruction $\epsilon_{\zeta ij}$ (1b) corresponding to the same scales as $\epsilon_{\epsilon ij}$. Both ζ_{ij} and $\epsilon_{\zeta ij}$ have a very weak shear component $(\cdot)_{xy}$ (Fig. 2). Their componentality obviously differs from that of $\{r_{ij}, \epsilon_{ij}, \epsilon_{\epsilon ij}\}$, because in the major part of the channel $(\cdot)_{xx} \approx (\cdot)_{yy} < (\cdot)_{zz}$ ($y^+ \gtrsim 10$; Fig. 2). Nonetheless, $\zeta_{yy} \rightarrow 0$ (2-C at the wall), contrary to $\epsilon_{\zeta yy}$ (Fig. 2), and in the sublayer $\epsilon_{\zeta xx}$ and $\epsilon_{\zeta zz}$ cross each other ($y^+ \lesssim 1$; Fig. 2), in analogy with the observed behaviour of $\epsilon_{\epsilon ij}$.

Regarding the acceleration correlations, a_{ij} (7c), $a_{ij}^{(p)}$ (7d) and $a_{ij}^{(v)}$ (7e), again the shear component is substantially smaller than the diagonal components (Fig. 2). Recall that the fluctuating momentum equation [5, (3.2b), p. 17]

$$\frac{Du'_i}{Dt} = -\frac{1}{\rho} \frac{\partial p'}{\partial x_i} + \nu \frac{\partial^2 u'_i}{\partial x_m \partial x_m} \quad (8a)$$

readily implies

$$(7c-8a) \implies a_{ij} = a_{ij}^{(p)} + a_{ij}^{(v)} - \frac{\nu}{\rho} \left(\frac{\partial p'}{\partial x_i} \frac{\partial^2 u'_j}{\partial x_k \partial x_k} + \frac{\partial p'}{\partial x_j} \frac{\partial^2 u'_i}{\partial x_m \partial x_m} \right) \quad (8b)$$

where the last cross-correlation tensor is symmetric but indefinite. The componentality of the acceleration correlations a_{ij} (7c) is quite different from that of its pressure $a_{ij}^{(p)}$ (7d) and viscous $a_{ij}^{(v)}$ (7e) parts, as these correlations are the footprint of different mechanisms occurring mainly at different scales. In the buffer layer ($10 \lesssim y^+ \lesssim 100$; Fig. 2) viscous acceleration is mainly in the streamwise direction, but in the sublayer $a_{zz}^{(v)}$ increases and crosses with $a_{xx}^{(v)}$ at $y^+ \approx 1$ (Fig. 2), in analogy with the other correlations between components of the fluctuating velocity Hessian, $\epsilon_{\epsilon ij}$ (7a) and $\epsilon_{\zeta ij}$ (1b). The wall normal component $a_{yy}^{(v)}$ becomes comparable to the other diagonal components only sufficiently away from the wall ($y^+ \gtrsim 30$; Fig. 2). On the other hand, acceleration induced by fluctuating pressure forces $a_{ij}^{(p)}$ (7d) exhibits a $a_{zz}^{(p)} > a_{yy}^{(p)} > a_{xx}^{(p)}$ anisotropy in the buffer layer ($10 \lesssim y^+ \lesssim 100$; Fig. 2), whereas near the wall $a_{yy}^{(p)} \rightarrow 0$ ($y^+ \lesssim 10$; Fig. 2). Finally, the acceleration correlations behave quite differently from the 2 parts in the fluctuating momentum equation (8a), implying that the cross-term in (8b) is important, and especially so near the wall where scale-separation tends to disappear, and is directly responsible for the differences in limiting behavior (Fig. 2)

$$\lim_{y^+ \rightarrow 0} a_{ij} = 0 \quad (8c)$$

$$\lim_{y^+ \rightarrow 0} a_{ij}^{(p)} \neq 0 \quad (8d)$$

$$\lim_{y^+ \rightarrow 0} a_{ij}^{(v)} \neq 0 \quad (8e)$$

More precise information on the componentality of these positive-definite symmetric tensors (1, 7) is obtained by considering their anisotropy invariant mapping (AIM) in the (III, -II)-plane (Fig. 3). Only r_{ij} (1a), ϵ_{ij} (1b), ζ_{ij} (1c) and a_{ij} (7c) are 2-C at the wall (Fig. 3). The fluctuating acceleration correlations a_{ij} (7c) reach the 2-C state near, although not exactly at, the axisymmetric disk-like boundary (Fig. 3). The tensors representing correlations between components of the fluctuating velocity Hessian, $\epsilon_{\epsilon ij}$ (7a), $\epsilon_{\zeta ij}$ (1b) and $a_{ij}^{(v)}$ (7e), invariably reach the axisymmetric disk-like boundary of the realizability triangle very near $y^+ \approx 1$ (Fig. 3), roughly where the streamwise $(\cdot)_{xx}$ and spanwise $(\cdot)_{zz}$ components cross each other (Fig. 2), and then return inside the realizability triangle as they approach the wall (Fig. 3). Near the centerline, a_{ij} approaches disk-like axisymmetry (Fig. 3), contrary to $a_{ij}^{(p)}$ (7d) and $a_{ij}^{(v)}$ (7e), both of which are axisymmetric rod-like (Fig. 3). The difference is that $a_{xx} < a_{yy} \approx a_{zz} \forall y^+ \gtrsim 50$ (Fig. 2), whereas $a_{xx}^{(p)} > a_{yy}^{(p)} \approx a_{zz}^{(p)} \forall y^+ \gtrsim 80$ (Fig. 2). Finally $a_{ij}^{(p)}$ approaches the 2-C boundary without reaching it, and then returns inside the realizability triangle (Fig. 3). Notice that by (8a, 8c) $[a_{ij}^{(p)}]_w = [a_{ij}^{(v)}]_w$ at the wall.

5 Conclusion

The simple algebraic proof presented above, can be summarized in the following mathematical proposition:

Theorem (Lumley's realizability triangle). Let \mathbf{r} be a real rank-2 Cartesian tensor in the 3-D Euclidean space \mathbb{E}^3 . Assume \mathbf{r} symmetric and positive definite. Then the locus of the invariants (2b) of the corresponding anisotropy tensor \mathbf{b}_r (2b), in the (III $_{\mathbf{b}_r}$, -II $_{\mathbf{b}_r}$)-plane, lies within Lumley's realizability triangle (6). \square

The proof (§3) follows directly from the well-known fact that the principal values of \mathbf{r} are real and nonnegative. By its algebraic nature it leads directly to the inequality (6), which defines Lumley's realizability triangle. It is obtained in the actual (III $_{\mathbf{b}_r}$, -II $_{\mathbf{b}_r}$)-plane, with no need of transformation of the invariants or explicit analysis of the limit states at the boundaries of the realizability triangle. The novel algebraic proof reported in the paper helps to better grasp the classic geometric proof given in Lumley [9].

Many symmetric tensors with nonnegative diagonal values are encountered in the analysis of turbulent flows. Several, by no means exhaustive, examples are studied, using DNS data for plane channel flow, illustrating how anisotropy invariant mapping (AIM) within the realizability triangle can improve our understanding of their componentality behavior.

Acknowledgements

The authors are listed alphabetically. The present work was partly supported by the ANR project N_{um}ERICCS (ANR-15-CE06-0009).

References

- [1] Bernard PS, Berger BS (1982) A method for computing 3-d turbulent flows. *SIAM J Appl Math* 42(3):453–470
- [2] Gerolymos GA, Vallet I (2005) Mean-flow-multigrid for implicit Reynolds-stress-model computations. *AIAA J* 43(9):1887–1898
- [3] Gerolymos GA, Vallet I (2009) Implicit mean-flow-multigrid algorithms for Reynolds-stress-model computations of 3-D anisotropy-driven and compressible flows. *Int J Num Meth Fluids* 61(2):185–219, DOI 10.1002/fld.1945
- [4] Gerolymos GA, Vallet I (2016) Comparison of reynolds-stress r_{ij} and dissipation ϵ_{ij} tensors budgets in turbulent plane channel flow. *Int J Heat Fluid Flow* [submitted 21 sep 2016; preprint *ArXiv* (2016) 1609.06512; <http://arxiv.org/pdf/1609.06512v1>]
- [5] Gerolymos GA, Vallet I (2016) The dissipation tensor ϵ_{ij} in wall turbulence. *J Fluid Mech* [doi:10.1017/jfm.2016.610; preprint *ArXiv* (2016) 1602.05022; <http://arxiv.org/pdf/1602.05022v3>]
- [6] Girimaji SS (2006) Partially-averaged Navier-Stokes model for turbulence: A Reynolds-averaged Navier-Stokes to direct numerical simulation bridging method. *ASME J Appl Mech* 73:422–429
- [7] Harris JW, Stocker H (1998) *Handbook of Mathematics and Computational Science*. Springer Verlag, New York [NY, USA]
- [8] Lee MJ, Reynolds WC (1987) On the structure of homogeneous turbulence. In: Durst F, Launder BE, Lumley JL, Schmidt FW, Whitelaw JH (eds) *Turbulent Shear Flows 5, Selected Papers for the 5. International Symposium on Turbulent Shear Flows*, Cornell University, Ithaca [NY, USA], aug, 7–9, 1985, Springer, Berlin [DEU], pp 54–66
- [9] Lumley JL (1978) Computational modeling of turbulent flows. *Adv Appl Mech* 18:123–176
- [10] Lumley JL, Newman GR (1977) The return to isotropy of homogeneous turbulence. *J Fluid Mech* 82:161–178
- [11] Schumann U (1977) Realizability of Reynolds-stress turbulence models. *Phys Fluids* 20:721–725
- [12] Segel LA (2007) *Mathematics Applied to Continuum Mechanics*. SIAM, Philadelphia [PA, USA], (unabridged republication of the MacMillan 1977 edition)
- [13] Simonsen AJ, Krogstad PÅ (2005) Turbulent stress invariant analysis: Classification of existing terminology. *Phys Fluids* 17:088103
- [14] Speziale CG (1998) Turbulence modeling for time-dependent RANS and VLES: A review. *AIAA J* 36(2):173–184
- [15] Stewart GW (1998) *Matrix Algorithms I*. SIAM, Philadelphia [PA, USA]
- [16] Tennekes H, Lumley JL (1972) *A First Course in Turbulence*. MIT Press, Cambridge [MA, USA]
- [17] Yeo K, Kim BG, Lee C (2010) On the near-wall characteristics of acceleration in turbulence. *J Fluid Mech* 659:405–419, DOI 10.1017/S0022112010002557
- [18] Yeung PK, Pope SB, Lamorgese AG, Donzis DA (2006) Acceleration and dissipation statistics in numerically simulated isotropic turbulence. *Phys Fluids* 18:065103